

Article

Daytime Land Surface Temperature Extraction from MODIS Thermal Infrared Data under Cirrus Clouds

Xiwei Fan ^{1,2}, Bo-Hui Tang ^{1,3}, Hua Wu ^{1,3}, Guangjian Yan ^{4,*} and Zhao-Liang Li ^{5,6,*}

¹ State Key Laboratory of Resources and Environment Information System, Institute of Geographic Sciences and Natural Resources Research, Chinese Academy of Sciences, Beijing 100101, China; E-Mails: fanxw.11b@igsrr.ac.cn (X.F.); tangbh@igsrr.ac.cn (B.-H.T.); wuhua@igsrr.ac.cn (H.W.)

² University of Chinese Academy of Sciences, Beijing 100049, China

³ Jiangsu Center for Collaborative Innovation in Geographical Information Resource Development and Application, Nanjing 210023, China

⁴ State Key Laboratory of Remote Sensing Science, School of Geography, Beijing Key Laboratory for Remote Sensing of Environment and Digital Cities, Beijing Normal University, Beijing 100875, China

⁵ Key Laboratory of Agri-informatics, Ministry of Agriculture/Institute of Agricultural Resources and Regional Planning, Chinese Academy of Agricultural Sciences, Beijing 100081, China

⁶ ICube, UdS, CNRS, 300 Bld Sebastien Brant, CS10413, Illkirch 67412, France

* Authors to whom correspondence should be addressed; E-Mails: gjyan@bnu.edu.cn (G.Y.); lizhaoliang@caas.cn (Z.-L.L.); Tel.: +86-10-6488-9277 (Z.-L.L.); Fax: +86-10-6488-9684 (Z.-L.L.).

Academic Editor: Assefa M. Melesse

Received: 9 March 2015 / Accepted: 23 April 2015 / Published: 28 April 2015

Abstract: Simulated data showed that cirrus clouds could lead to a maximum land surface temperature (LST) retrieval error of 11.0 K when using the generalized split-window (GSW) algorithm with a cirrus optical depth (*COD*) at 0.55 μm of 0.4 and in nadir view. A correction term in the *COD* linear function was added to the GSW algorithm to extend the GSW algorithm to cirrus cloudy conditions. The *COD* was acquired by a look up table of the isolated cirrus bidirectional reflectance at 0.55 μm . Additionally, the slope *k* of the linear function was expressed as a multiple linear model of the top of the atmospheric brightness temperatures of MODIS channels 31–34 and as the difference between split-window channel emissivities. The simulated data showed that the LST error could be reduced from 11.0 to 2.2 K. The sensitivity analysis indicated that the total errors from all the uncertainties of

input parameters, extension algorithm accuracy, and GSW algorithm accuracy were less than 2.5 K in nadir view. Finally, the Great Lakes surface water temperatures measured by buoys showed that the retrieval accuracy of the GSW algorithm was improved by at least 1.5 K using the proposed extension algorithm for cirrus skies.

Keywords: cirrus clouds; error correction; generalized split-window algorithm; land surface temperature retrieval; MODIS

1. Introduction

Land surface temperature (LST) is an important parameter because of its control on the upward terrestrial radiation and the energy exchange between the Earth's surface and the atmosphere [1,2]. Satellite remote sensing offers the only possibility to measure LST over extended regions with high temporal and spatial resolutions [3]. However, because of the complex influences of cirrus clouds on atmospheric radiative transfer and relatively low atmospheric transmittances, the current LST retrieval algorithms using satellite thermal-infrared (TIR) data typically do not consider the influences of cirrus clouds and therefore are only applied for clear-sky conditions.

Cirrus clouds, which are relatively optically thin, have a global coverage of approximately 20%, with over 60%–70% in the tropics [4], and a thin cirrus layer may be present as much as 80% of the time in tropical regions [5]. It has been noted that globally distributed high and thin cirrus clouds introduce serious retrieval difficulties of atmospheric temperature and humidity profiles and surface geophysical parameters from space-based platforms, owing to the semitransparency of these clouds at visible and infrared wavelengths [6–8]. Regarding the effects of cirrus clouds on estimates of sea surface temperature (SST), Xu and Sun [8] indicated an error of 1.5–2.0 K on SST retrieval occurs if clear-sky SST retrieval equations were used in the presence of cirrus. Additionally, Fan *et al.* [9] indicated using simulated data that the maximum LST error raised to approximately 12 K in the vertical view when the generalized split-window (GSW) algorithm was used in LST retrieval under cirrus cloudy conditions.

To retrieve LST under cirrus-skies, Fan *et al.* [10] proposed a three-channel LST retrieval algorithm with considering the variations in cirrus optical depth (*COD*), cirrus effective radius (*R*), and cirrus top height (*CTH*) [11,12]. However, because the algorithm relies on the mid-infrared channel, the observations in the mid-infrared channel at satellite altitudes during the daytime consist of a combination of reflected radiance due to sun irradiance and emitted radiance from both the surface and the atmosphere and hence cannot be used to retrieve LST during the daytime. Thus, the algorithms aim to retrieve daytime SST or LST under cirrus skies are necessary. Because the GSW algorithm is one of the most efficient and commonly used methods to estimate LST from satellite TIR data with an accuracy of better than 1 K at nadir view [13], the objective of this work is to develop an algorithm to extend the clear-sky-based GSW algorithm to cirrus cloudy conditions with considering the variations of *COD*, *R*, and *CTH*.

The outline of this paper is as follows: Section 2 presents the data used in this study. Section 3 shows the influences of cirrus on LST retrieval and the extension algorithm to reduce those influences. Results

and some analyses are provided in Section 4. Section 5 presents the results for validating the proposed algorithm with field measurements and MODIS satellite data. Conclusions are presented in the final section.

2. Data

2.1. Simulated Datasets

The atmospheric radiative transfer code MODerate resolution atmospheric TRANsmission (MODTRAN) is used to simulate Top of the Atmosphere (TOA) radiances for methodology development. First, 60 clear-sky atmospheric profiles, 54 main land cover types [14] and cirrus optical properties of a general habit mixture (GHM) selected from radiosonde observation databases-Thermodynamic Initial Guess Retrieval (TIGR) database [15], Advanced Spaceborne Thermal Emission Reflection Radiometer (ASTER) spectral library [16], and Ice Cloud Bulk Scattering Models [17,18], respectively, are used in the simulations. The specific procedures for the selection of atmospheric profiles and land cover types from TIGR and ASTER, respectively, and a brief introduction of TIGR, ASTER and GHM are provided by [10].

Two simulated datasets, *Data-cirrus* and *Data-clearsky*, are produced to extend the GSW algorithm in cirrus skies, where the differences in the two dataset-estimated LSTs are considered as the influences of cirrus on LST retrieval. *Data-cirrus* contains the TOA radiances of MODIS channels 31–34 (centered at 11.0, 12.0, 13.4, and 13.7 μm) with considering the influences of cirrus clouds, and *Data-clearsky* contains the TOA radiances of split-window channels without considering such influences. As the detection limitation of the MODIS cloud mask products is approximately 0.4 for *COD* for the visible bands [19], namely the conventional clear-sky-based LST retrieval algorithms are commonly misused to retrieve LST under cirrus skies when the *COD* is less than 0.4, the slant path *COD* at 0.55 μm varies from 0.04 to 0.4 in steps of 0.04 in the production of *Data-cirrus*. Additionally, cirrus optical properties with an *R* greater than 15 μm are used in this study due to the lower occurrence probability of small particles in cirrus clouds [20]. Furthermore, the *CTH* are varied from 8 km to 16 km in steps 4 km [11]. To increase the representativeness of the simulations, reasonable variations of day-time LST are varied in a wide range from near surface atmospheric temperature (T_0) minus 5 K to T_0 plus 15 K in step of 5 K. By adding cirrus optical properties of different *R* into MODTRAN with *COD* (at 0.55 μm) being 0.04 to 0.4 and *CTH* being 8 km to 16 km, the cirrus influenced TOA radiances in four MODIS TIR channels are produced based on the clear-sky atmospheric profiles and land surface emissivities (LSEs) previously selected from TIGR and ASTER, respectively. Other detailed procedures for the production of *Data-cirrus* are referred to in [10]. The TOA brightness temperatures for the MODIS split-window channels in clear-sky conditions (*Data-clearsky*) are produced similarly as those for *Data-cirrus* for methodology development.

2.2. Satellite Data

Four MODIS products are used in the study: (1) Calibrated Radiances 5-Min L1B Swath 1-km dataset (MOD021KM/MYD021KM) in collection 6; (2) Geolocation Fields 5-Min L1A Swath 1-km dataset (MOD03/MYD03) in collection 6; (3) Clouds 5-Min L2 Swath 1-km dataset (MOD06_L2/MYD06_L2) in collections 5.1 and 6, respectively; and (4) Land Surface Temperature and Emissivity 5-Min L2 Swath

1-km dataset (MOD11_L2/MYD11_L2) in collection 5. Those products are saved in Hierarchical Data Format (HDF) and are available from NASA's Goddard Space Flight Center (GSFC) Level 1 and Atmosphere Archive and Distribution System (LAADS).

The observed radiances in channels 31–34 of the MOD021KM/MYD021KM dataset at a 1-km spatial resolution are used to acquire the corresponding TOA brightness temperatures for extending the GSW algorithm in cirrus cloudy conditions.

The MOD03/MYD03 dataset contains latitude and longitude, solar zenith and azimuth angles, and satellite viewing zenith and azimuth angles for every pixel at a 1-km spatial resolution. The latitude and longitude data are used to perform geometric corrections for three other 1-km resolution MODIS products used in this study. The solar and satellite viewing geometries are applied to convert cirrus reflectance into *COD*, and the satellite viewing zenith angles (VZAs) are used to determine the coefficients of the proposed extension algorithm.

The cloud mask products in MOD06_L2/MYD06_L2 are used to select the confident clear-sky pixels to eliminate the influences of other types of clouds on MOD11_L2/MYD11_L2 for method validations. Additionally, the isolated cirrus bidirectional reflectance (ICBR) and cirrus reflectance flag are used to determine the *COD* of cirrus in this study.

The LSTs are extracted from MOD11_L2/MYD11_L2 to compare with the results of the extended GSW algorithm in cirrus skies, and the corresponding LSEs in split-window channels are used to determine the correction term in the extension algorithm.

2.3. Study Area and Field Measurements

It is a difficult task to acquire the field measured true values of LST at satellite pixel scales due to the thermal inhomogeneity of the land surface compared with lake or sea surfaces. The water temperatures of the Great Lakes measured with buoys 45005 (41.677 °N, 82.398 °W), 45008 (44.283 °N, 82.416 °W), 45161 (43.178 °N, 86.361 °W) at 0.6 m under water and recorded by the Great Lakes CoastWatch Node (<http://coastwatch.glerl.noaa.gov/>) are used to represent the daytime MODIS pixel-scale lake surface water temperatures in this study. Additionally, the water temperatures measured with buoys 45137 (45.545 °N, 81.015 °W), 45139 (43.252 °N, 79.535 °W), 45143 (44.945 °N, 80.627 °W), 45147 (42.430 °N, 82.683 °W), 45149 (43.542 °N, 82.075 °W), and 45159 (43.767 °N, 78.983 °W) and recorded by Environment Canada are also used. Figure 1 is the MODIS/Terra true color map of the study area around Great Lakes on 6 May 2013 (MOD021KM.A2013126.1605.006.2013127012129); the locations of the nine buoys are also shown on this map. It can be seen that there are some thick clouds identified by the MODIS cloud mask product at the bottom left of this map; additionally, the thin clouds in the upper part of this map are used to validate the performance of the proposed extension algorithm.

The lake water temperatures measured by the nine buoys from May to November in 2013 with an accuracy of 0.1 K are collected in this study for algorithm validations. Note that the buoys measure the lake water temperatures with sample intervals of hourly averaged at most, and it meets the recommendations by Minnett [21] that the validation measurements should be made within ± 2 h of the satellite overpass. Furthermore, the buoys used in this study are located at least 1 km away from lakeshore to avoid the mixed land/lake surface pixels.

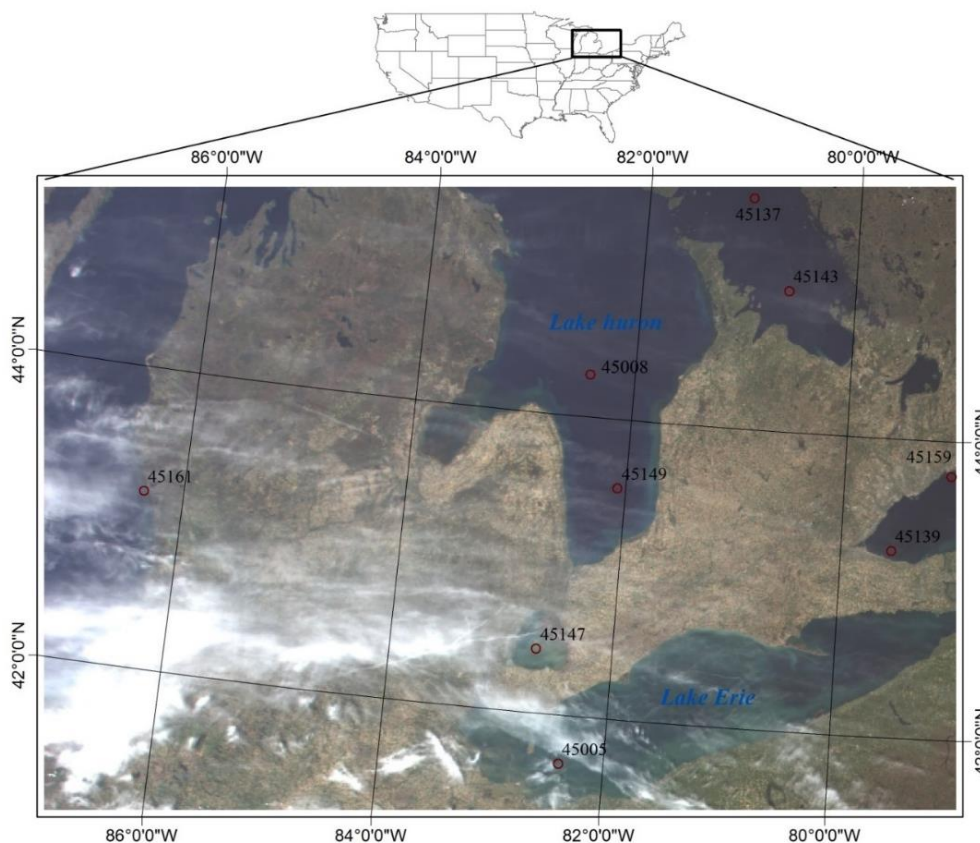


Figure 1. MODIS/Terra true color map of the study area around the Great Lakes on 6 May 2013 (MOD021KM.A2013126.1605.006.2013127012129) indicating the locations of the nine buoys selected in this study.

3. Method

3.1. LST Retrieval under Cirrus Clouds

The GSW algorithm extended from the physically based local split-window algorithm proposed by [22] is expressed as [23]:

$$LST = a_0 + \left(a_1 + a_2 \frac{1 - \varepsilon}{\varepsilon} + a_3 \frac{\Delta \varepsilon}{\varepsilon^2} \right) \frac{T_{31} + T_{32}}{2} + \left(a_4 + a_5 \frac{1 - \varepsilon}{\varepsilon} + a_6 \frac{\Delta \varepsilon}{\varepsilon^2} \right) \frac{T_{31} - T_{32}}{2} \quad (1)$$

where T_{31} and T_{32} are the TOA brightness temperatures of MODIS split-window channels, respectively; ε and $\Delta \varepsilon$ are the mean and difference of the split-window channel emissivities, respectively; the VZA dependent a_i ($i = 0-6$) are the numerical coefficients of the GSW algorithm.

To improve the LST retrieval accuracy, the GSW algorithm is divided into six groups according to the water vapor content (WVC) of the atmospheric profiles selected in the previous section with an overlap of 0.5 g/cm^2 : 0–1.5, 1.0–2.5, 2.0–3.5, 3.0–4.5, 4.0–5.5, 5.0–6.5 g/cm^2 [24]. Then, six groups of a_i ($i = 0-6$) coefficients in Equation (1) are determined for each VZA using the Levenberg-Marquardt statistical regression method from *Data-clearsky*. The LSTs with (LST_{COD}) and without ($LST_{clear-sky}$) including the influences of cirrus are retrieved from *Data-cirrus* and *Data-clearsky*, respectively, in the GSW algorithm using the coefficients. Note that the errors in LST_{COD} are the sums of the GSW algorithm errors and the errors caused by cirrus, and the errors in $LST_{clear-sky}$ are only from GSW algorithm errors,

which are irregular for further process. Thus, similar as estimating the influences of dust aerosol on LST retrieval in the GSW algorithm [25], the following equation is used to estimate the influences of cirrus clouds on the retrieval of LST (ΔT_{COD}):

$$\Delta T_{COD} = LST_{COD} - LST_{clear-sky}, (0.04, \dots, 0.4) \quad (2)$$

where ΔT_{COD} is calculated from the corresponding pairs of LST_{COD} and $LST_{clear-sky}$ for each COD from 0.04 to 0.4. Figure 2 shows the biases and standard deviations (STDs) of ΔT_{COD} versus COD at $0.55 \mu\text{m}$ for three example VZAs, indicating that cirrus clouds lead to an underestimation of the LST retrieved using the GSW algorithm with a bias of -1.2 K with $COD = 0.04$ and $VZA = 0^\circ$. Both the STD of ΔT_{COD} and the absolute value of the bias increase as the COD increases. The STD and bias reach up to 4.1 K and -12.8 K , respectively, when $COD = 0.4$ and $VZA = 60^\circ$.

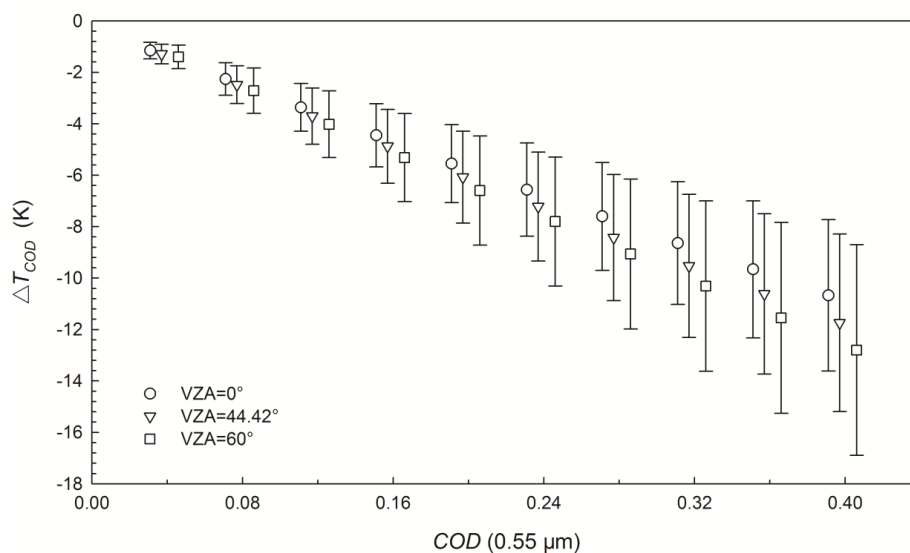


Figure 2. Influence of cirrus clouds on LST retrieval (ΔT_{COD}) using the GSW algorithm with simulated MODIS data for three VZAs. The hollow symbols indicate the biases and the half-length of vertical bars represent the STDs of ΔT_{COD} calculated with Equation (2).

The biases of ΔT_{COD} in Figure 2 indicate that the COD is one of the primary factors that determine LST retrieval errors because of its dominant influence on cirrus transmittances in split-window channels. Thus, inspired by the extension of the GSW algorithm under dust aerosol skies [25], the LST retrieval accuracy of the GSW algorithm under cirrus skies can be improved using the following correction term:

$$\Delta T_{COD} = k * COD, (COD \leq 0.4) \quad (3)$$

where k is the slope varying with LSE, CTH , R and VZA . The offset of Equation (3) is 0 because the LST retrieval errors are 0 without the presence of cirrus. The mean, STD, and maxima of the root mean square errors (RMSEs) between the actual ΔT_{COD} calculated with Equation (2) and the ΔT_{COD} regressed based on Equation (3) for the vertical view condition are 0.13, 0.06, and 0.7 K, respectively, which indicates that the proposed linear function can appropriately correct for the LST retrieval error of the GSW algorithm caused by cirrus. Thus, k and COD are necessary to Equation (3) for extending the GSW algorithm under cirrus skies.

3.2. Determination of Slope k

The determination of slope k in Equation (3) is necessary to improve the retrieval accuracy of the GSW algorithm under cirrus skies. Because the difference between LST and the cirrus temperature (T_c) is a dominant factor for the reduction in the split-window channel TOA brightness temperatures for a given COD , the temperature difference between LST and the cirrus temperature ($T_s - T_c$) is used to obtain k . Additionally, because the cirrus effective radius controls the differences of cirrus transmittances in split-window channels [26], R is also employed to calculate k . Furthermore, the emissivity difference in split-window channels is also considered to determine k . Figure 3 presents the relationships between k and $T_s - T_c$, R , and $\Delta\varepsilon$ in the simulated dataset as an example. The slope k can be expressed as a linear function of $T_s - T_c$ and $\Delta\varepsilon$ and a quadratic function of R . Considering the effects of those factors, a multiple regression model is used to determine the value of k :

$$k = 31.79 - 0.26*(T_s - T_c) - 2.02*R + 0.02*R^2 - 85.22\Delta\varepsilon \quad (4)$$

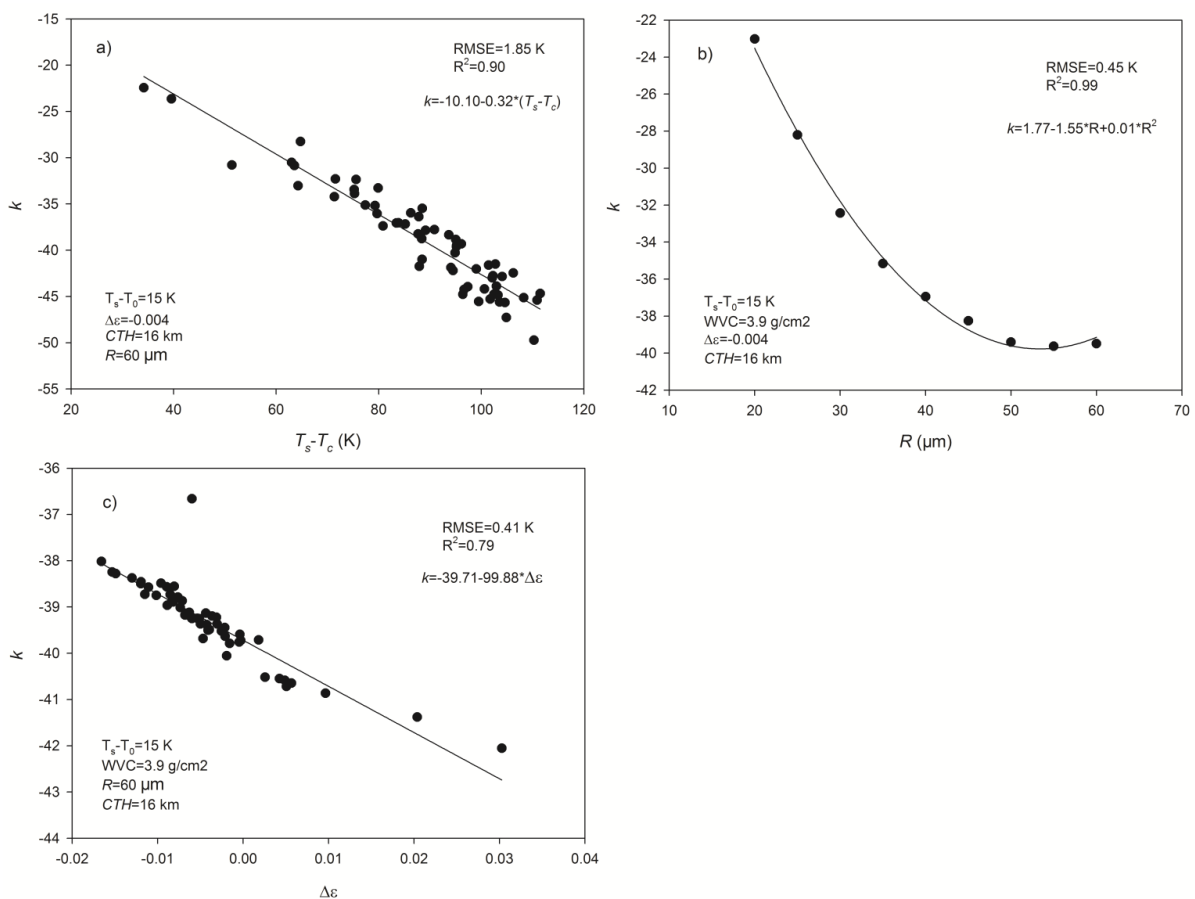


Figure 3. The relationships between slope k in Equation (3) and (a) the difference between LST and cirrus temperature ($T_s - T_c$); (b) the cirrus effective radius (R); (c) the difference of the split-window channel emissivities ($\Delta\varepsilon$).

The coefficients in Equation (4) are determined from the previously simulated dataset in nadir view with the Levenberg-Marquardt statistical regression method. The RMSE between the estimated k and the actual value is 3.2 K, and the coefficient of determination (R^2) of the fitting equation is 0.92,

indicating that Equation (4)-calculated k can be used to correct for the influences of cirrus on LST retrieval with $\Delta T_{COD} - k \cdot COD$ and after correction the RMSE of ΔT_{COD} becomes approximately 1.3 K ($3.2 \text{ K} \times 0.4$) in nadir view when the COD at $0.55 \mu\text{m}$ is 0.4. Additionally, because the a_i ($i = 0-6$) coefficients of the GSW algorithm in Equation (1) depend on the VZA, the biases in Figure 2 are affected slightly by VZA. Therefore, the VZA must also be considered in the determination of slope k when correcting for ΔT_{COD} .

Considering MODIS channels 33 and 34 are commonly related with atmospheric temperature profiles [27], the TOA brightness temperature differences between channels 31 and 34 ($T_{31} - T_{34}$) and between 31 and 33 ($T_{31} - T_{33}$) are employed to substitute $T_s - T_c$. Because the differences in the TOA brightness temperatures in split-window channels are related to the effective radius of cirrus [26], $T_{31} - T_{32}$ is also employed to estimate k . Thus, a new multiple linear regression model is used to determine the value of k to replace Equation (4):

$$k = k_0 + k_1(T_{31}-T_{34}) + k_2(T_{31}-T_{33}) + k_3(T_{31}-T_{32}) + k_4\Delta\varepsilon \quad (5)$$

where k_i ($i = 0-4$) are the statistical regression coefficients dependent on VZA, which are shown in Table 1. The RMSEs between the estimated and actual k for different VZAs are also shown in Table 1. The minimum and maximum RMSEs of Equation (5)-estimated k are 5.67 and 8.33 K for VZA = 0° and 60° , respectively, leading to LST errors of 2.26 and 3.33 K when COD is 0.4. These results indicate that after $T_s - T_c$ and R are substituted with $T_{31} - T_{34}$, $T_{31} - T_{33}$, and $T_{31} - T_{32}$, the LST errors after correction increase by approximately 1 K when VZA = 0° . The value of k_i ($i = 0-4$) can be interpolated by secant VZA for the VZAs not included in Table 1.

Table 1. Values of coefficients k_0 , k_1 , k_2 , k_3 and k_4 in Equation (5) for six VZAs.

| Secant(VZA) | k_0 (K) | k_1 | k_2 | k_3 | k_4 (K) | RMSE (K) |
|-------------|-----------|-------|-------|-------|-----------|----------|
| 1.0 | -17.57 | 0.67 | -1.39 | -1.09 | -37.85 | 5.67 |
| 1.2 | -20.38 | 0.97 | -1.73 | -1.48 | -27.90 | 6.41 |
| 1.4 | -21.37 | 0.92 | -1.58 | -2.21 | -13.11 | 7.01 |
| 1.6 | -22.28 | 0.92 | -1.51 | -2.74 | -3.18 | 7.47 |
| 1.8 | -22.86 | 0.89 | -1.44 | -3.18 | 4.47 | 7.87 |
| 2.0 | -22.84 | 0.72 | -1.16 | -3.8 | 12.92 | 8.33 |

3.3. Determination of COD

The MODIS 1.375- μm channel is a strong water vapor absorption band, and the reflectance essentially is caused by the reflection and scattering of cirrus clouds because of the relatively small attenuation by the water vapor above and within cirrus and small sensitivity to the lower level water clouds and to the surface. Using the 1.375 μm “cirrus detection” band, the ICBR at visible wavelength, what is free of surface reflection and atmospheric effects and is independent of cloud mask algorithm, is produced as part of MODIS cloud products-MOD06_L2/MYD06_L2 [28].

A look up table (LUT) of the ICBR at different COD , solar and satellite viewing geometries are constructed with MODTRAN to acquire COD . A total of 4864 solar and satellite viewing geometries in this LUT are considered with solar and satellite VZAs increasing from 0° to 75° at intervals of 5° and relative azimuth angles varying from 0° to 180° at intervals of 10° . Additionally, because the cloud

reflectance in the visible channel is sensitive to COD but insensitive to R [29], the cirrus optical properties when R is 20 μm in the GHM is used in the simulation with a slant path COD at 0.55 μm varying from 0.04 to 0.4 in steps of 0.04. The atmospheric WVC and surface reflectance are both 0 in the simulation to eliminate the influences of the atmosphere and the land surface. The differences in the TOA reflectance at 0.55 μm between cirrus-sky and clear-sky conditions then are taken as the ICBR. The COD can be determined with the inversion of the LUT with the ICBR at given solar and satellite viewing geometries, and the cirrus cloudy pixels can be discriminated from actual clear-sky pixels simultaneously with a COD greater than 0.02 [30] and a cirrus reflectance flag of “cirrus”. The procedure for the construction of this LUT is shown in Figure 4.

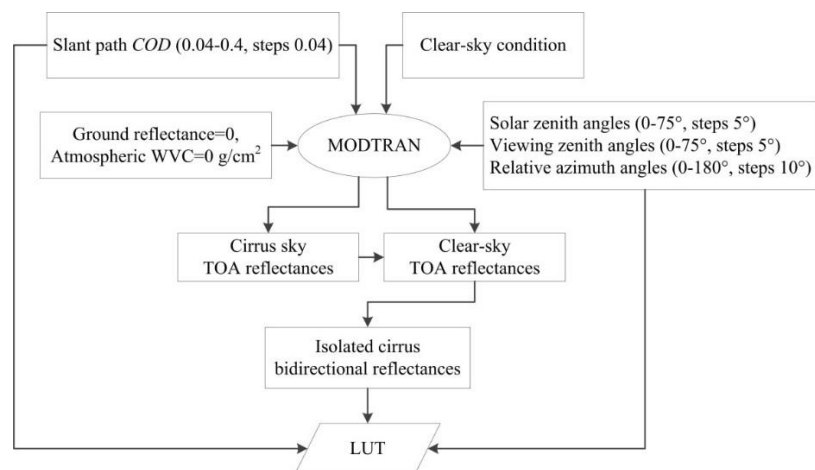


Figure 4. Procedure for the generation of the ICBR LUT.

4. Results and Analysis

4.1. Results

Using the COD that can be interpolated from the ICBR LUT in actual applications, and with the slope k determined from TOA brightness temperatures in MODIS channels 31–34 and split-window channel emissivities, the LST retrieve accuracy of the GSW algorithm under cirrus skies is improved using the correction term $LST_{COD} - k * COD = LST_{AC}$. Figure 5 shows the RMSEs between the LST_{COD} and $LST_{clear-sky}$ (hollow symbols) and the RMSEs between the LST_{AC} and $LST_{clear-sky}$ (solid symbols). The RMSE is 1.2 K with a COD of 0.04 and a VZA of 0°, increasing to 13.4 K with a COD of 0.4 and a VZA of 60° without correction. Figure 5 also indicates that the RMSE increases slightly with increasing VZA and COD after correction; the maximum RMSE between LST_{AC} and $LST_{clear-sky}$ is 3.2 K when the COD at 0.55 μm is 0.4 and a VZA of 60°.

Figure 6 shows histograms of ΔLST from $\Delta LST = \Delta T_{COD} - k * COD$ when the COD at 0.55 μm are 0.04, 0.2, and 0.4, respectively. The ΔLST is mainly between ± 1 K when the COD is 0.04. The ΔLST varies between -6 and 4 K for VZA = 0° with a COD of 0.4 and between -7 and 5 K for VZA = 60°. The bias is -0.8 K after correction compared to -12.8 K before correction when COD is 0.4 and VZA is 60°. It is clear from this figure that the proposed extension algorithm can improve the retrieval accuracy of the GSW algorithm under cirrus skies significantly.

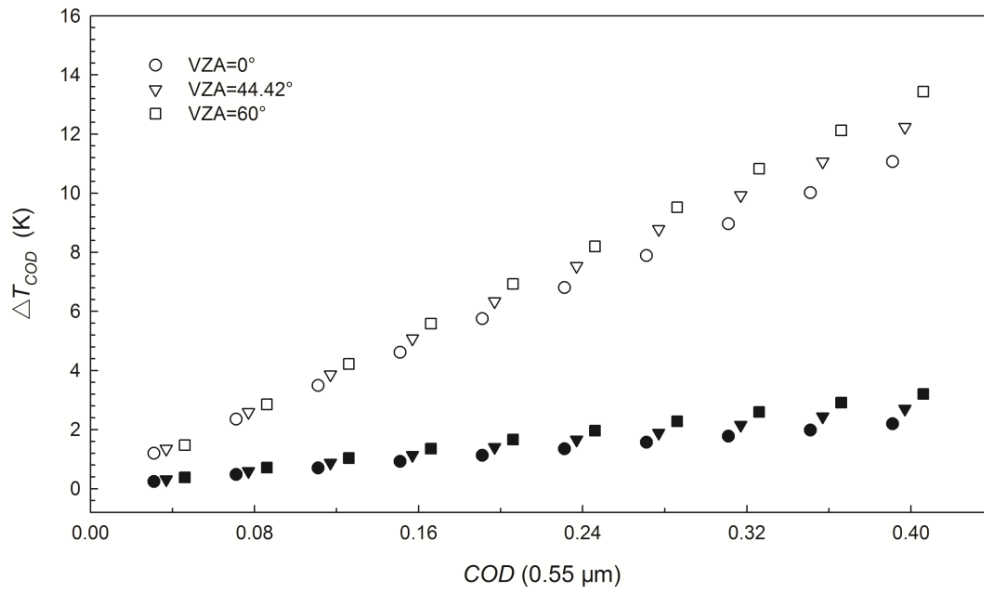


Figure 5. RMSEs between the $LST_{clear-sky}$ and LST_{COD} (hollow symbols) and the RMSEs between the $LST_{clear-sky}$ and LST_{AC} (solid symbols) for three VZAs. LST_{COD} and $LST_{clear-sky}$ are those retrieved from *Data-cirrus* and *Data-clearsky* using the GSW algorithm, respectively. LST_{AC} are the LSTs of LST_{COD} minus the correction term $k*COD$.

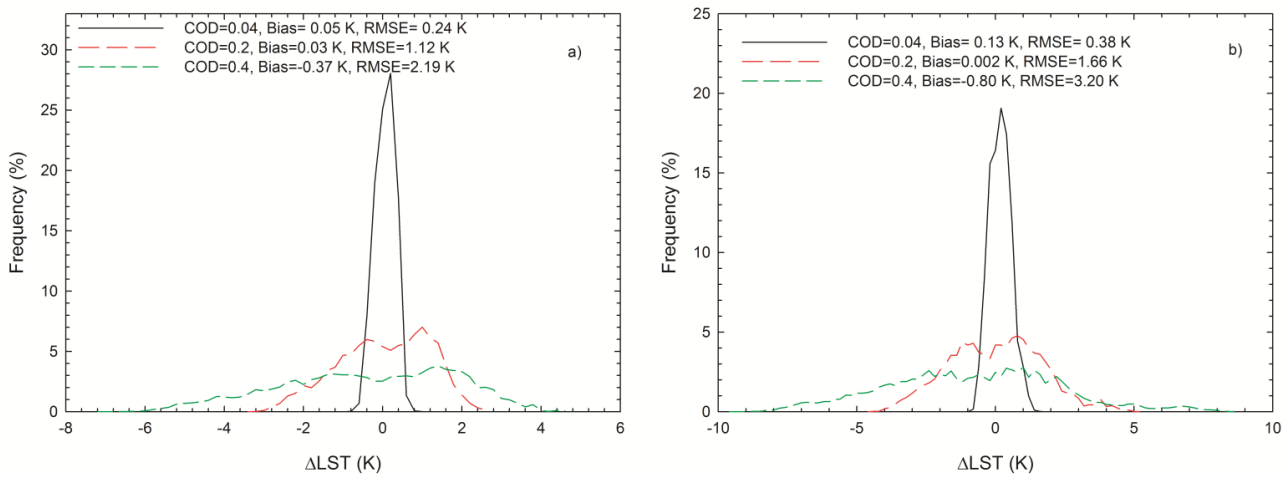


Figure 6. Histograms of LST errors after correction ($\Delta LST = \Delta T_{COD} - k*COD$) with a COD (at $0.55 \mu m$) = 0.04, 0.2 and 0.4 for (a) $VZA = 0^\circ$ and (b) $VZA = 60^\circ$.

4.2. Analysis

The uncertainty of the proposed GSW extension algorithm for cirrus cloudy conditions is evaluated with a sensitivity analysis. Additionally, the total errors of the extended GSW algorithm-retrieved LST ($\delta(LST_{AC})$) is a combination of the extension algorithm accuracy ($\delta(LST_A)$), the errors associated with the uncertainties of the input parameters ($\delta(LST_P)$), and the accuracy of the GSW algorithm ($\delta(LST_{GSW})$):

$$\delta(LST_{AC}) = \sqrt{\delta(LST_A)^2 + \delta(LST_P)^2 + \delta(LST_{GSW})^2} \tag{6}$$

with:

$$\delta(LST_p) = \sqrt{\delta(T_{34})^2 + \delta(T_{33})^2 + \delta(T_{32})^2 + \delta(T_{31})^2 + \delta(\Delta\varepsilon)^2 + \delta(COD)^2} \quad (7)$$

where:

$$\delta(T_i) = \left| \frac{\partial \Delta T_{COD}}{\partial T_i} \Delta T_i \right|, \quad (i = 31, 32, 33, \text{ or } 34) \quad (8)$$

$$\delta(\Delta\varepsilon) = \left| \frac{\partial \Delta T_{COD}}{\partial \Delta\varepsilon} \Delta\varepsilon \right| \quad (9)$$

$$\delta(COD) = |k * \Delta(COD)| \quad (10)$$

where ΔT_i ($i = 31, 32, 33, \text{ or } 34$), $\Delta(\Delta\varepsilon)$, and $\Delta(COD)$ are the uncertainties of T_i , $\Delta\varepsilon$, and COD , respectively; the $\delta(T_i)$ ($i = 31, 32, 33, \text{ or } 34$), $\delta(\Delta\varepsilon)$, and $\delta(COD)$ are the LST errors caused by ΔT_i , $\Delta(\Delta\varepsilon)$, and $\Delta(COD)$, respectively.

The RMSEs between LST_{AC} and $LST_{clear-sky}$ as the solid symbols show in Figure 5 are taken as $\delta(LST_A)$. The accuracy of the COD ($\Delta(COD)$) derived from cirrus reflectance is approximately 0.02 [30]. Because the LST errors from the uncertainties of COD are multiplied by k as in Equation (10), the mean slope of the biases versus COD in Figure 2 is used to determine $\delta(COD)$. Then, the $\delta(COD)$ are 0.53 and 0.61 K for $VZA = 0^\circ$ and 60° , respectively. Considering MODIS instrument errors of 0.25 K for channels 34 and 33 and 0.05 K for channels 32 and 31, a typical error of 0.01 for $\Delta\varepsilon$, and 1 K for $\delta(LST_{GSW})$ [13], the $\delta(T_i)$ ($i = 31, 32, 33, \text{ or } 34$), $\delta(\Delta\varepsilon)$, and $\delta(LST_{AC})$ in vertical view are shown in Figure 7 with solid symbols. Additionally, the $\delta(LST_{AC})$ when $VZA = 44.42^\circ$ and 60° are also shown in Figure 7 with hollow triangles and hollow rectangles, respectively.

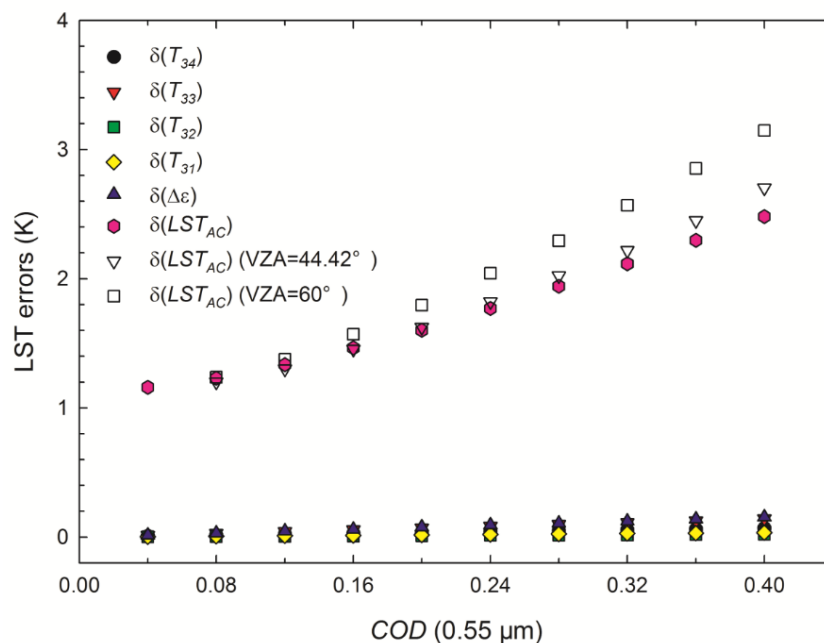


Figure 7. LST errors of $\delta(T_i)$ ($i = 31, 32, 33, \text{ and } 34$) and $\delta(\Delta\varepsilon)$ caused by the uncertainties of T_i and $\Delta\varepsilon$, respectively, and the total LST errors ($\delta(LST_{AC})$) in vertical view versus COD at $0.55 \mu\text{m}$ (solid symbols). $\delta(LST_{AC})$ when $VZA = 44.42^\circ$ and 60° is shown in hollow triangles and hollow rectangles, respectively.

The LST errors $\delta(T_{31})$, $\delta(T_{32})$, $\delta(T_{33})$, $\delta(T_{34})$, and $\delta(\Delta\varepsilon)$ in Figure 7 as a result of the uncertainties in T_{31} , T_{32} , T_{33} , T_{34} , and $\Delta\varepsilon$ are all less than 0.2 K, indicating that the LST errors from the uncertainties of COD are larger compared with the errors from other input parameter uncertainties. Additionally, the total LST errors $\delta(LST_{AC})$ increase with increases in COD because the error of the extension algorithm is the dominant factor in the total LST errors. The maxima of $\delta(LST_{AC})$ are 2.5 and 3.4 K for $VZA = 0^\circ$ and 60° , respectively.

Because the constant coefficients in the GSW algorithm cannot be used for worldwide LST retrievals under various atmospheric profiles [22] or land surface conditions, the GSW algorithm is commonly divided into several sub-ranges according to atmospheric WVC, LSE, T_0 (or LST). However, the atmospheric WVC estimates may be inaccurate because of the changes in the TOA reflectance of the atmospheric WVC retrieval bands due to the presence of cirrus [31]. In addition to the uncertainties discussed above, the LST errors as a result of the misapplication of the GSW algorithm due to inaccurate input of atmospheric WVC is not considered in this study.

COD is a vital factor in identifying and correcting for LST errors in the GSW algorithm under cirrus skies. However, the accuracy of COD may decrease in some extreme dry atmospheric conditions, such as over desert areas, because the MODIS “cirrus detection” channel can be contaminated slightly by lower level water clouds and bright surfaces. Thus, the performance of the extension algorithm in those regions may not be as accurate as in humid atmospheric regions or on dark surfaces, such as over lake or sea surfaces. Fortunately, the probability of cirrus occurrence is low in dry atmospheres [11].

The values of $T_s - T_c$ and R are substituted with a multiple linear model of TOA brightness temperatures of MODIS channels 31 to 34 to acquire the slope k for actual applications. The accuracy of the extension algorithm decreases by approximately 1 K when Equation (5) is used to determine k compared with using the Equation (4)-calculated k . The difference in cirrus transmittances in split-window channels is one of the dominant factors in the difference in corresponding channel TOA brightness temperatures and is determined by the cirrus effective radius R . To acquire more accurate LST under cirrus-skies, the values of R or a more accurate substitute for R for the extended GSW algorithm can be used in the following on study.

5. Validations

Assuming the buoy-measured lake water temperatures (LST_{buoy}) are equivalent to the lake surface water temperatures, the MODIS LST uncertainties can be computed as the differences between LST products-MOD11_L2/MYD11_L2 and LST_{buoy} . The COD is interpolated with the LUT constructed in the previous section using the ICBR in MOD06_L2/MYD06_L2 and the solar and satellite viewing geometries in MOD03/MYD03 to improve the retrieval accuracy of the GSW algorithm under cirrus skies using the extension algorithm. Additionally, k is determined from TOA brightness temperatures calculated from MOD021KM/MYD021KM of channels 31–34 and with split-window channel emissivities extracted from MOD11_L2/MYD11_L2. The pixels labeled as confident clear sky in MOD06_L2/MYD06_L2, interpolated COD greater than 0.02 and the cirrus reflectance flag as “cirrus” are considered as cirrus-sky pixels to eliminate the influences from other cloud types; the differences between MOD11_L2/MYD11_L2 and LST_{buoy} are determined then as the LST errors caused by cirrus that can be reduced using the correction term of MOD11_L2/MYD11_L2 minus $k \cdot COD$ (LST_{AC}).

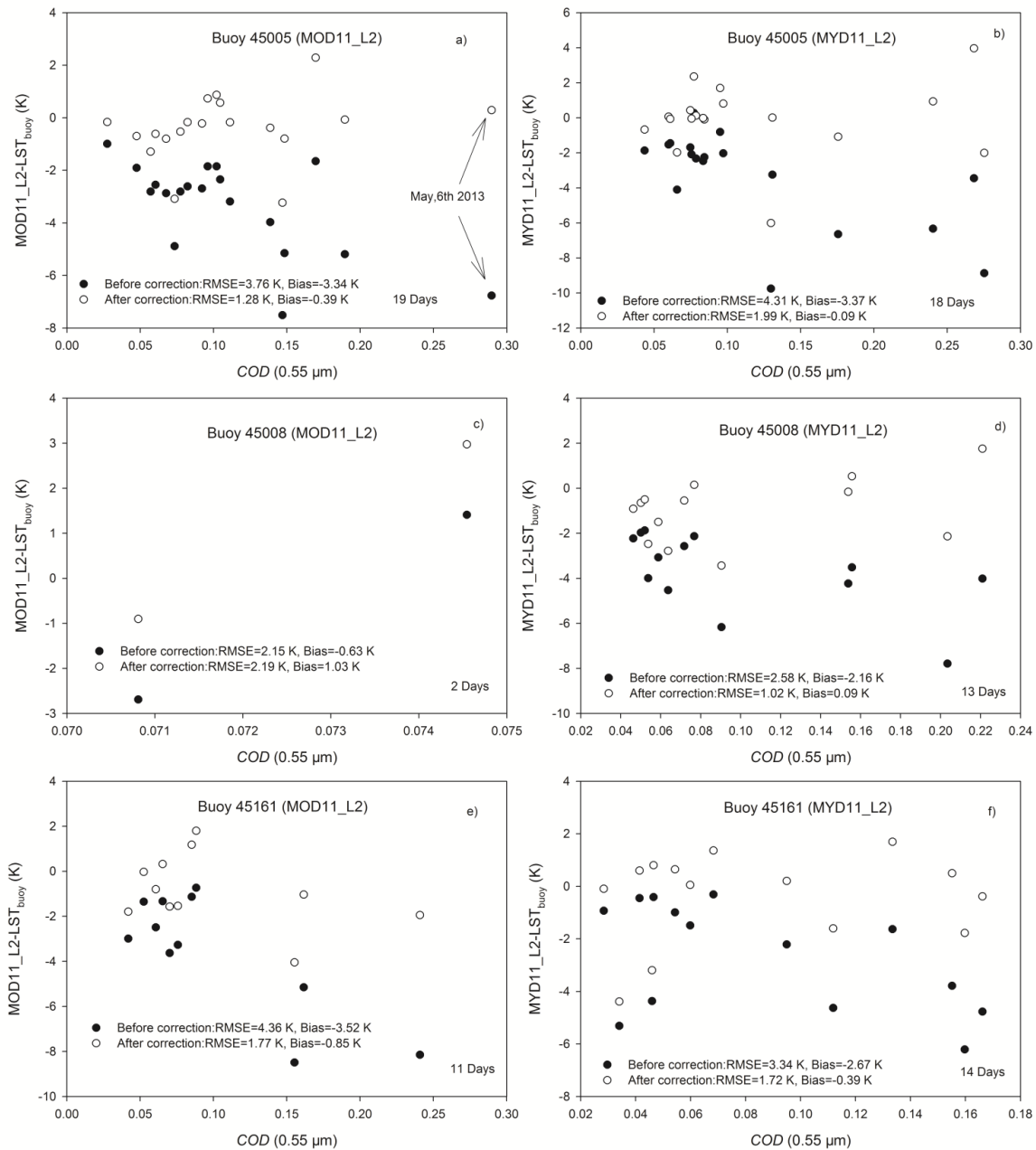


Figure 8. LST differences between LSTs extracted from MOD11_L2/MYD11_L2 and LST_{buoy} (solid circles) and between the LST_{AC} and LST_{buoy} (hollow circles) versus COD (at $0.55 \mu m$) for three different buoys from May to November 2013. (a,b) show the result of MOD11_L2/MYD11_L2 at buoy 45005, respectively; (c,d) show the result of MOD11_L2/MYD11_L2 at buoy 45008, respectively; (e,f) show the result of MOD11_L2/MYD11_L2 at buoy 45161, respectively.

Figure 8 shows the LST differences between LSTs extracted from MOD11_L2/MYD11_L2 and LST_{buoy} (solid circles) and between the LST_{AC} and LST_{buoy} (hollow circles) versus COD at $0.55 \mu m$ for buoys 45005, 45008, and 45161, respectively. The MODIS LSTs retrieved using the clear-sky-based GSW algorithm tend to be underestimated when COD increases, and the retrieval accuracy of the GSW algorithm under cirrus skies can be improved using the correction term. The RMSEs of MODIS LSTs at buoy 45005 are 1.28 and 1.99 K after correction for MOD11_L2 and MYD11_L2, respectively,

compared with the RMSEs of 3.76 and 4.31 K before correction; similar results are also shown in Figure 8c–f for buoys 45008 and 45161. Except for the MOD11_L2 at buoy 45008 (not considered because it includes only two days), the RMSEs of MODIS LSTs after correction are less than half of the original RMSEs before correction. The proposed algorithm can improve the retrieval accuracy of the GSW algorithm under cirrus skies by at least 1.5 K for buoy 45008 with MYD11_L2 data, and the maximum improvement is 2.6 K for buoy 45161 with MOD11_L2 data. The correction results of the remaining six buoys are shown in Table 2.

Because some of the buoys were malfunctioning from May to November in 2013, a majority of the available validation samplings are less than 5 days (except 45143/MYD11_L2 has 9 days) for the six buoys. Seven of the RMSEs or biases (eleven in all) in Table 2 decrease after correction compared with the RMSEs without correction; however, the remaining four RMSEs tend to increase. The RMSEs are unstable and can be influenced heavily by the correction performance of individual samples due to the small number of available validation samplings. Thus, the validation results in Table 2 do not precisely reflect the performance of the proposed extension algorithm in actual applications.

Table 2. Biases and RMSEs of LST errors before and after error correction for buoys 45137, 45139, 45143, 45147, 45149, and 45159. The data are collected from May to November 2013.

| Data | Days | MOD11_L2/ MY11_L2 | | LST_{AC} | |
|----------------|------|-------------------|----------|------------|----------|
| | | Bias (K) | RMSE (K) | Bias (K) | RMSE (K) |
| 45137/MOD11_L2 | 0 | - | - | - | - |
| 45137/MYD11_L2 | 5 | -2.94 | 3.49 | 2.05 | 4.68 |
| 45139/MOD11_L2 | 4 | -4.71 | 5.67 | -3.37 | 4.88 |
| 45139/MYD11_L2 | 3 | -3.19 | 3.26 | -0.35 | 1.10 |
| 45143/MOD11_L2 | 3 | -2.10 | 2.28 | 1.71 | 3.40 |
| 45143/MYD11_L2 | 9 | -1.54 | 1.67 | 1.55 | 3.44 |
| 45147/MOD11_L2 | 5 | -5.77 | 6.05 | 0.35 | 2.34 |
| 45147/MYD11_L2 | 1 | -1.95 | - | 1.36 | - |
| 45149/MOD11_L2 | 1 | -4.09 | - | 0.52 | - |
| 45149/MYD11_L2 | 2 | -0.93 | 1.75 | -0.09 | 1.24 |
| 45159/MOD11_L2 | 1 | -2.85 | - | 4.20 | - |
| 45159/MYD11_L2 | 3 | -2.76 | 3.52 | -1.15 | 1.89 |

For example, 6 May 2013 in Figure 9 shows the (a) Terra/MODIS true color map of the study area, (b) ICBR in MOD06_L2, (c) COD at $0.55 \mu\text{m}$ where the COD is greater than 0.02 and less than 0.4, the cirrus reflectance flags are “cirrus”, and the corresponding LSTs in MOD11_L2 are available, (d) LST errors estimated using the proposed extension algorithm ($k * COD$), (e) MOD11_L2, and (f) MOD11_L2 after correction (LST_{AC}). The maximum value of the LSTs increases from 313 K in MOD11_L2 to 317 K for LST_{AC} after correction, and the surface water temperatures of Lake Huron shown in the red rectangle (Figure 9a) are more homogeneous after correction (Figure 9f) compared with MOD11_L2 (Figure 9e). Eight buoy-measured lake water temperatures when MODIS/Terra observed on 6 May 2013 are shown in Table 3 to study the correction performance of the proposed extension algorithm shown in Figure 9. The corresponding pixel COD at $0.55 \mu\text{m}$, the lake surface water temperatures in MOD11_L2 and LST_{AC} are also shown in Table 3. Because there is no LST value in MOD11_L2 at buoy 45008, its

result is no shown in this Table. The LST_{AC} tend to be more close to LST_{buoy} compared with MOD11_L2. The RMSE and bias between LST_{AC} and LST_{buoy} in Table 3 are 1.2 and 0.4 K, respectively and 5.5 and -4.0 K between MOD11_L2 and LST_{buoy} .

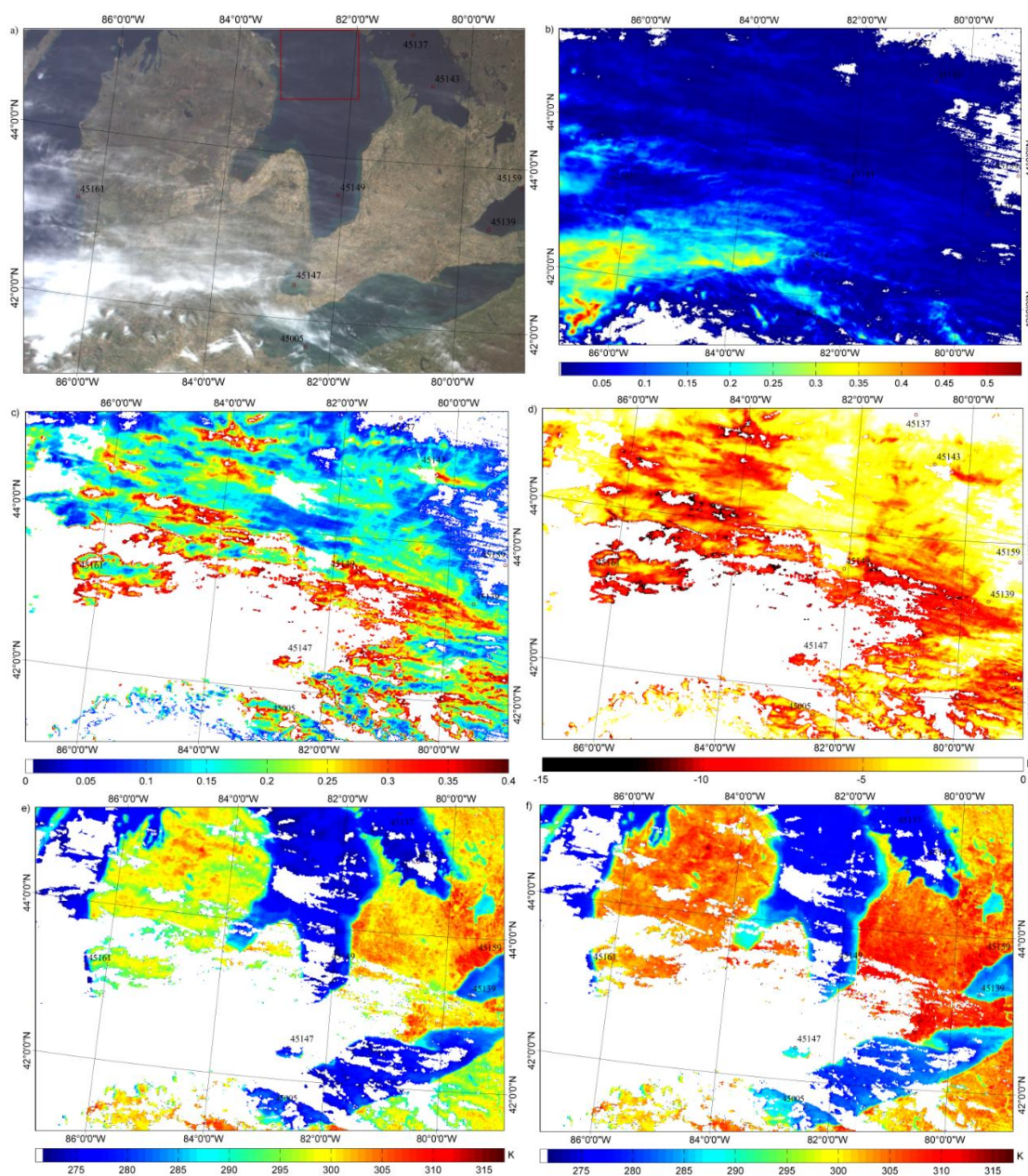


Figure 9. (a) Terra/MODIS true color map of the study area, (b) ICBR in MOD06_L2, (c) COD at $0.55 \mu\text{m}$ where the COD is greater than 0.02 and less than 0.4, the cirrus reflectance flags are “cirrus”, and the corresponding LSTs in MOD11_L2 are available, (d) LST errors estimated using the proposed extension algorithm ($k*COD$), (e) MOD11_L2, and (f) MOD11_L2 corrected with $k*COD$.

Table 3. Buoy locations and buoy-measured lake water temperature (LST_{buoy}) for MODIS/Terra observations on 6 May 2013; cirrus optical depth (COD) at $0.55 \mu\text{m}$, MODIS/Terra LST products-MOD11_L2, and MOD11_L2 after correction (LST_{AC}) for the pixels where the buoys are located.

| Buoy | Latitude (°) | Longitude (°) | LST_{buoy} (K) | COD | MOD11_L2 (K) | LST_{AC} (K) |
|-------|--------------|---------------|------------------|-------|--------------|----------------|
| 45005 | 41.677 | -82.398 | 282.45 | 0.28 | 275.68 | 282.74 |
| 45137 | 45.545 | -81.015 | 276.85 | 0 | 276.90 | 276.90 |
| 45139 | 43.252 | -79.535 | 284.25 | 0.14 | 282.22 | 285.80 |
| 45143 | 44.945 | -80.627 | 276.55 | 0.19 | 273.14 | 277.50 |
| 45147 | 42.430 | -82.683 | 286.85 | 0.39 | 276.10 | 287.03 |
| 45149 | 43.542 | -82.075 | 276.55 | 0.16 | 275.40 | 278.96 |
| 45159 | 43.767 | -78.983 | 281.45 | 0 | 281.40 | 281.40 |
| 45161 | 43.178 | -86.361 | 282.25 | 0.24 | 274.10 | 280.34 |

Additionally, the COD at buoys 45137 and 45159 are both 0 where the LSTs in MOD11_L2 are the same as the corresponding LSTs in LST_{AC} , where the biases of MOD11_L2 at the corresponding buoys are 0.05 and -0.05 K, respectively. This result indicates that the proposed extension algorithm can improve the retrieval accuracy of the GSW algorithm in cirrus skies and can discriminate actual clear-sky conditions from cirrus skies accurately.

Figure 10a,b shows the histogram of the COD in Figure 9c and the histogram of the LST errors $k*COD$ in Figure 9d, respectively. Assuming the correction accuracy (the RMSEs are 5.5 and 1.2 K for MOD11_L2 and LST_{AC} , respectively) of the eight spatially scattered buoys can represent the correction performance of the available pixels in Figure 9d, then it can also be assumed that the clear-sky-based GSW algorithm is commonly misused for the retrieval of LST in cirrus skies with a mean and STD of cirrus COD at $0.55 \mu\text{m}$ of 0.19 and 0.08, respectively; and as a result, the LSTs are underestimated with the mean and STD of -5.06 and 2.44 K, respectively. Figure 7 indicates that the total LST errors after correction are 1.5 and 2.0 K when $VZA = 0^\circ$ and 60° , respectively, for a COD of 0.2. Hence, LSTs with a mean error of 1.5–2.0 K can be acquired under cirrus cloudy conditions using the proposed extended GSW algorithm.

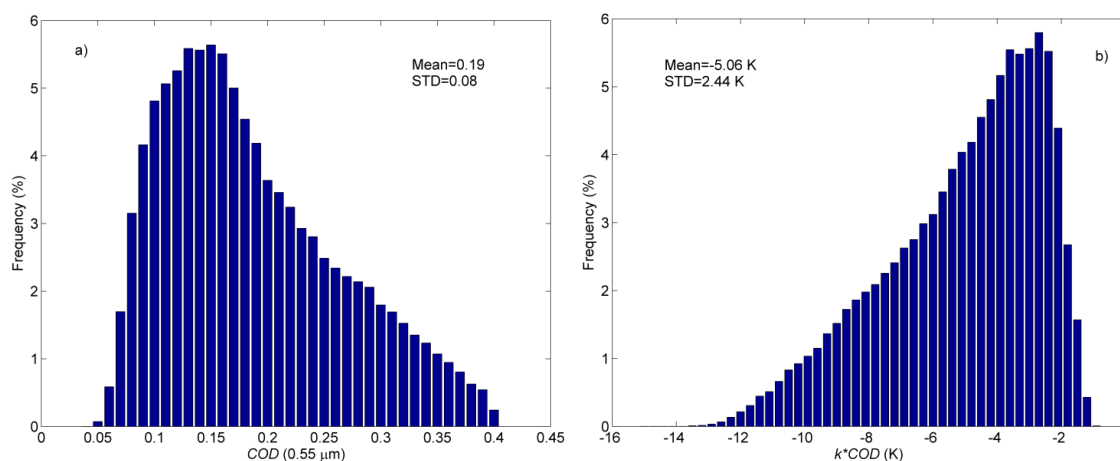


Figure 10. Histograms of (a) COD at $0.55 \mu\text{m}$ in Figure 9c and (b) LST errors estimated using the proposed extension algorithm ($k*COD$) in Figure 9d.

6. Conclusions

Conventional LST retrieval algorithms from TIR data are developed and applied for clear-sky conditions, and the influences of cirrus clouds are not considered in their development. To study the influences of cirrus clouds on LST retrieval, two different simulated datasets (with and without including the influences of cirrus clouds) were used to retrieve LSTs using the GSW algorithm with the same coefficients obtained from the later dataset. The differences between the two groups of retrieved LSTs indicated that the maximum RMSE was 11.0 K when the COD at $0.55 \mu\text{m}$ was 0.4 and in nadir view.

An extension algorithm is proposed by adding a correction term in function of COD in the GSW algorithm to improve the retrieval accuracy in cirrus cloudy conditions. A LUT of the ICBR at $0.55 \mu\text{m}$ was established with MODTRAN for different COD , solar and satellite viewing geometries to acquire COD . Then, the COD at $0.55 \mu\text{m}$ was determined with an inversion of the LUT for a given ICBR in the MODIS cloud products, and the cirrus-sky pixel was discriminated from actual clear-sky simultaneously. Additionally, the slope k of the linear function was expressed as a multiple linear model of the TOA brightness temperature differences between MODIS channels 31 and 34 ($T_{31} - T_{34}$), 31 and 33 ($T_{31} - T_{33}$), 31 and 32 ($T_{31} - T_{32}$), and the difference between split-window channel emissivities ($\Delta\varepsilon$). The simulated data indicated that the LST error caused by cirrus was reduced from 11.0 to 2.2 K after correction using the proposed extension algorithm.

The LST errors caused by the uncertainties in the input variables T_{34} , T_{33} , T_{32} , T_{31} , $\Delta\varepsilon$, and COD were analyzed to study the uncertainty of the proposed extension algorithm in cirrus skies. The LST errors from MODIS instrument noise and $\Delta\varepsilon$ were less than 0.2 K, and the errors from COD were approximately 0.6 K. The total LST errors of the extended GSW algorithm caused by the uncertainties of the input parameters, extension algorithm accuracy, and the GSW algorithm accuracy were also analyzed. The results showed that the total LST errors increased with increasing COD , and the maximum total LST error was 2.5 K for $COD = 0.4$ and $VZA = 0^\circ$.

The buoy-measured lake water temperatures in the Great Lakes were used to validate the performance of the proposed extension algorithm for LST retrievals. The validations showed that the proposed extension algorithm could improve the retrieval accuracy of the GSW algorithm by at least 1.5 K under cirrus skies, or more than half of the original RMSE values before correction.

Note that in addition to MODIS, other satellite TIR data-retrieved LSTs under cirrus skies, such as Suomi-NPP/VIIRS or Landsat-8/(OLI and TIRS) that equipped with a cirrus detection band, can also be corrected using this algorithm even with a constant slope k . This algorithm can be used not only for improving LST retrieval accuracy but also to improve the SST-retrieve accuracy under cirrus with a higher accuracy.

Acknowledgments

This work was jointly supported by the National Natural Science Foundation of China under grant 41171287 and 41231170, the National High Technology Research and Development Program of China under grant 2012AA121103, the Excellent Young Talent Funds for Kezhen Distinguished Young Scholar in the Institute of Geographic Sciences and Natural Resources Research (IGSNRR), Chinese

Academy of Sciences (CAS) under grant 2012RC101, and the International Science & Technology Cooperation Program of China under Grant 2014DFE10220.

Author Contributions

Xiwei Fan, Bo-Hui Tang and Zhao-Liang Li developed the overall approach. Zhao-Liang Li and Xiwei Fan contributed to the methodological development and programming. Hua Wu and Guangjian Yan conducted the in-situ data processing. Xiwei Fan and Bo-Hui Tang prepared the manuscript.

Conflicts of Interest

The authors declare no conflict of interest.

References

1. Lu, J.; Tang, R.; Tang, H.; Li, Z.-L. A new parameterization scheme for estimating surface energy fluxes with continuous surface temperature, air temperature, and surface net radiation measurements. *Water Resour. Res.* **2014**, *50*, 1245–1259.
2. Duan, S.-B.; Li, Z.-L.; Tang, B.-H.; W, H.; Tang, R. Direct estimation of land-surface diurnal temperature cycle model parameters from MSG–SEVIRI brightness temperatures under clear sky conditions. *Remote Sens. Environ.* **2014**, *150*, 34–43.
3. Li, Z.-L.; Tang, B.-H.; Wu, H.; Ren, H.; Yan, G.; Wan, Z.; Trigo, I.F.; Sobrino, J.A. Satellite-derived land surface temperature: Current status and perspectives. *Remote Sens. Environ.* **2013**, *131*, 14–37.
4. Wylie, D.P.; Menzel, W.P.; Woolf, H.M.; Strabala, K.I. Four years of global cirrus cloud statistics using HIRS. *J. Clim.* **1994**, *7*, 1972–1986.
5. Wang, P.-H.; McCormick, M.P.; Poole, L.R.; Chu, W.P.; Yue, G.K.; Kent, G.S.; Skeens, K.M. Tropical high cloud characteristics derived from SAGE II extinction measurements. *Atmos. Res.* **1994**, *34*, 53–83.
6. Sassen, K.; Cho, B.S. Subvisual/thin cirrus dataset for satellite verification and climatological research. *J. Appl. Meteorol.* **1992**, *31*, 1275–1285.
7. Liou, K.-N. Influence of cirrus clouds on weather and climate processes: A global perspective. *Mon. Weather Rev.* **1986**, *114*, 1167–1199.
8. Xu, L.; Sun, B. Influence of cirrus clouds on the VISSR atmospheric sounder-derived sea surface temperature determinations. *Appl. Opt.* **1991**, *30*, 1525–1536.
9. Fan, X.; Tang, B.-H.; Wu, H.; Tang, R.; Yan, G.; Li, Z.-L. Influence of thin cirrus clouds on land surface temperature retrieval using the generalized split-window algorithm from thermal infrared data. In Proceedings of 2014 IEEE International Geoscience and Remote Sensing Symposium (IGARSS), Quebec City, QC, Canada, 13–18 July 2014; pp. 3037–3040.
10. Fan, X.; Tang, B.-H.; Wu, H.; Yan, G.; Li, Z.-L. A three-channel algorithm for retrieving nighttime land surface temperature from MODIS data under thin cirrus clouds. *Int. J. Remote Sens.* **2015**, in press.

11. Nazaryan, H.; McCormick, M.P.; Menzel, W.P. Global characterization of cirrus clouds using CALIPSO data. *J. Geophys. Res.* **2008**, *113*, doi:10.1029/2007JD009481.
12. Sassen, K.; Wang, Z.; Liu, D. Global distribution of cirrus clouds from CloudSat/Cloud-Aerosol Lidar and Infrared Pathfinder Satellite Observations (CALIPSO) measurements. *J. Geophys. Res.* **2008**, *113*, doi:10.1029/2008JD009972.
13. Wan, Z. New refinements and validation of the MODIS land-surface temperature/emissivity products. *Remote Sens. Environ.* **2008**, *12*, 59–74.
14. Li, Z.-L.; Wu, H.; Wang, N.; Qiu, S.; Sobrino, J.A.; Wan, Z.; Tang, B.-H.; Yan, G. Land surface emissivity retrieval from satellite data. *Int. J. Remote Sens.* **2013**, *34*, 3084–3127.
15. Chedin, A.; Scott, N.A.; Wahiche, C.; Moulinier, P. The improved initialization inversion method: A high resolution physical method for temperature retrievals from satellites of the TIROS-N series. *J. Clim. Appl. Meteorol.* **1985**, *24*, 128–143.
16. Baldridge, A.M.; Hook, S.J.; Grove, C.I.; Rivera, G. The ASTER spectral library version 2.0. *Remote Sens. Environ.* **2009**, *44*, 711–715.
17. Baum, B.A.; Yang, P.A.; Heymsfield, J.; Platnick, S.; King, M.D.; Hu, Y.-X.; Bedka, S.T. Bulk scattering properties for the remote sensing of ice clouds. Part II: Narrowband models. *J. Appl. Meteorol.* **2005**, *44*, 1896–1911.
18. Baum, B.A.; Yang, P.; Heymsfield, A.J.; Bansemer, A.; Merrelli, A.; Schmitt, C.; Wang, C. Ice cloud bulk single-scattering property models with the full phase matrix at wavelengths from 0.2 to 100 μm . *J. Quant. Spectrosc. Radiat. Transf.* **2014**, *146*, 123–139.
19. Ackerman, S.A.; Holz, R.E.; Frey, R.; Eloranta, E.W.; Maddux, B.C.; McGill, M. Cloud detection with MODIS. Part II: Validation. *J. Atmos. Ocean. Technol.* **2008**, *25*, 1073–1086.
20. Michael, M.D.; Platnick, S.; Menzel, W.P.; Ackerman, S.A.; Hubanks, P.A. Spatial and temporal distribution of clouds observed by MODIS onboard the Terra and Aqua satellites. *IEEE Trans. Geosci. Remote Sens.* **2013**, *51*, 3826–3852.
21. Minnett, P.J. Consequences of sea surface temperature variability on the validation and applications of satellite measurements. *J. Geophys. Res.* **1991**, *96*, 18475–18489.
22. Becker, F.; Li, Z.-L. Towards a local split window method over land surfaces. *Int. J. Remote Sens.* **1990**, *11*, 369–393.
23. Wan, Z.; Dozier, J. A generalized split-window algorithm for retrieving land-surface temperature from space. *IEEE Trans. Geosci. Remote Sens.* **1996**, *34*, 892–905.
24. Tang, B.-H.; Bi, Y.; Li, Z.-L.; Xia, J. Generalized split-window algorithm for estimate of land surface temperature from Chinese Geostationary FengYun Meteorological Satellite (FY-2C) data. *Sensors* **2008**, *8*, 933–951.
25. Fan, X.; Tang, B.-H.; Wu, H.; Yan, G.; Li, Z.-L.; Zhou, G.; Shao, K.; Bi, Y. Extension of the generalized split-window algorithm for land surface temperature retrieval to atmospheres with heavy dust aerosol loading. *IEEE J. Sel. Top. Appl. Earth Obs. Remote Sens.* **2015**, *8*, 825–834.
26. Parol, F.; Buriez, J.C.; Brogniez, G.; Fouquart, Y. Information content of AVHRR channels 4 and 5 with respect to the effective radius of cirrus cloud particles. *J. Appl. Meteorol.* **1991**, *30*, 973–984.
27. Tang, B.-H.; Li, Z.-L. Estimation of instantaneous net surface longwave radiation from MODIS cloud-free data. *Remote Sens. Environ.* **2008**, *112*, 3482–3492.

28. Gao, B.-C.; Yang, P.; Han, W.; Li, R.-R.; Wiscombe, W.J. An algorithm using visible and 1.38- μm channels to retrieve cirrus cloud reflectances from aircraft and satellite data. *IEEE Trans. Geosci. Remote Sens.* **2002**, *40*, 1659–1668.
29. Nakajima, T.; King, M.D. Determination of the optical thickness and effective particle radius of clouds from reflected solar radiation measurements. Part I: Theory. *J. Atmos. Sci.* **1990**, *47*, 1878–1893.
30. Dessler, A.E.; Yang, P. The distribution of tropical thin cirrus clouds inferred from Terra MODIS data. *J. Clim.* **2003**, *16*, 1241–1247.
31. Gao, B.-C.; Kaufman, Y.J. Water vapor retrievals using moderate resolution Imaging spectroradiometer (MODIS) near-infrared channels. *J. Geophys. Res.* **2003**, *108*, doi:10.1029/2002JD003023.

© 2015 by the authors; licensee MDPI, Basel, Switzerland. This article is an open access article distributed under the terms and conditions of the Creative Commons Attribution license (<http://creativecommons.org/licenses/by/4.0/>).